1 **An unusual inverted saline microbial mat community in an interdune sabkha in the Rub' al**
2 **Khali (the Empty Quarter), UAE: An analog for habitats on present Mars.**
3

4 Christopher P. McKay[1], Jon C. Rask[1], Angela M. Detweiler[1,2], Brad M. Bebout[1], R. Craig
5 Everroad[1,2], Jackson Z. Lee[1,2], Jeffrey P. Chanton[3], Marisa H. Mayer[1], Adrian A. L. Caraballo[1],
6 Bennett Kapili[1], Meshgan Al-Awar[4], and Asma Al-Farraj[5]
7

8 [1]NASA Ames Research Center, Moffett Field CA 94035
9

10 [2]Bay Area Environmental Research Institute, Petaluma, CA 94952
11

12 [3]Department of Earth, Ocean and Atmospheric Science, Florida State University, Tallahassee,
13 FL 32306-4320, United States
14

15 [4]Research and Studies Center, Dubai Police Academy, Dubai, United Arab Emirates
16

17 [5]Geography Department, United Arab Emirates University, P.O. Box 17771, Al Ain, United
18 Arab Emirates
19

20 Corresponding author: Chris.McKay@NASA.gov
21

22 Draft of 12 Jan 2016
23 Revised for PLOS One
24

25

Abstract

Salt flats (sabkha) are a recognized habitat for microbial life in desert environments and as analogs for habitats for life on Mars. Here we report on the physical setting and microbiology of interdune sabkhas among the large dunes in the Rub' al Khali (the Empty Quarter) in Liwa Oasis, United Arab Emirates. The salt flats, composed of gypsum and halite, between the dunes are moistened by relatively fresh ground water from below. The result is a salinity gradient that is inverted compared to most salt flat communities with the hypersaline layer at the top and freshwater layers below. We describe and characterize a rich photosynthetically-based microbial ecosystem that is protected from the arid outside environment below the translucent salt crust. Gases collected from sediments under shallow ponds in the sabkha contain methane in concentrations as high as 3400 ppm. The salt layer provides environmental protection to the habitat below and could preserve biomarkers and other evidence for life in the salt after it dries out. Chloride-filled depressions have been identified on Mars and although the surface flow of water is unlikely on Mars today, ground water is possible. Such a near surface system with modern groundwater flowing under ancient salt deposits could be present on Mars and could be accessed by surface rovers.

Introduction

Hypersaline environments are often found in deserts where intense evaporation and low levels of water input create concentrations of salt. Such environments are of interest as examples of life in extremes and are also relevant to the question of life on Mars – a cold desert world. Salt flats are relevant analogs for habitats for life on Mars both because salt can stabilize water as liquid at low temperature and pressure and because a salt crust can preserve evidence of past life. Accordingly, there has been considerable discussion of the relevance of coastal salt flats of marine origin as possible environments for life on Mars and as sites of preservation of biomarkers [14,36,37,42]. Desert salt flats have been studied as well. Davila et al. [9] reported on hydroscopic salts trapping atmospheric water to supply photosynthetic microbes in salt domes in the driest regions of the Atacama Desert [43]. Douglas and coworkers [11, 12, 13] conducted a series of studies in the mineralogical and microbiological properties of the Badwater salt flat in Death Valley, California. Barbieri et al. [5] considered organic preservation and biosignatures in dry salt flats of gypsum from Upper Pleistocene evaporite deposits of the Chott el Gharsa, a wide continental "sabkha" (a transliteration of the Arabic word for a salt flat) in southern Tunisia. Coastal sabkha are present along the Arabian Gulf (a.k.a. the Persian Gulf) along the northern coastline of the United Arab Emirates (UAE) [1,17] as subtidal flats, intertidal flats, and in particular as extensive supratidal flats [40]. There are also sabkhas deep inland in the UAE in the Liwa Oasis within the dunes of the Rub' al Khali (the Empty Quarter) which is an extensive area of aeolian dunes covering much of the Arabian Peninsula, including part of the UAE and eastern Saudi Arabia [16]. Small basins between the dunes connect to the water table, creating a flat level below which aeolian deflation cannot readily occur [16]. The interdune flats may be sites of erosion or deposition, and may be classified according to moisture content as dry, damp, wet, or evaporitic [16] and can contain salt crusts [15,16, 51]. These inland sabkha are an interesting analog for salt deposits on Mars and are the focus of this study.

Salt deposits are important targets in the search for life on Mars. Recent orbital data have indicated brine deposits associated with the seasonal dark streaks on Mars known as recurring slope lineae [27]. The indicated salts are calcium perchlorate and magnesium perchlorate. However chloride salts are expected on Mars as well. Orbital spectral data indicates that there are chloride-bearing deposits, likely formed in an evaporitic environment in the ancient geologic regions of Mars [10,30,31]. The surface conditions at these locations are currently too dry to support life and the pressure is too low to allow liquid water. The deposits on Mars are at the low levels in the basin but the elevation is high, 1260 m [10]. The inland sabkhas of the Liwa Oasis may be an analog for how these Martian salt flats could support life just below the surface in the present climate of Mars.

The hydrology of the Liwa Oasis has been well-studied because the shallow aquifer is an important source of fresh water for human use. Thus, the age and structure of the aquifer, the flow and composition of the groundwater, and the nature of the salt flats, are well-described [2,49-54] and summarized briefly here. The location of the Liwa Oasis is shown in Figure 1. The landscape is dominated by large sand dunes with interdune spaces [15,16,19]. The sand is deposited on a flat layer of middle Miocene-age carbonates, which is essentially at sea level [51]. The aquifer contains water that is held in the sand dunes bounded below by the impermeable carbonate layer [51]. This is shown schematically in Figure 2. The water table crests in the interior of the dune field and slopes downward following the topography of the dunes, as shown in Figure 2. Flow lines are shown as solid arrows and evaporation is indicated as wavy arrows. In the interdune areas, particularly near the edge of the dune field, the level of the ground water can reach the surface and wet surfaces are produced. Over time these wet areas accumulate solutes from evaporation and a salt flat (sabkha) is formed - as indicated in Figure 2. Radiocarbon dating and models of the groundwater formation for the Liwa Oasis [51] imply that the groundwater formed when the rainfall was approximately 20±5 cm/yr between 6,200 and 9,000 yr before present and that the shift from wet to dry took place relatively rapidly between 5,500 and 6,200 yr ago. The 1990 predevelopment elevations of this water table are reported at 105 m for the crest and 85 m for the locations of discharge near the edges of the sand dunes [51]. The composition of the salts in the ground water is dominated by $CaSO_4$ and NaCl [51]. Measurements of the Cl content of the groundwater near the crest of the aquifer [51] indicated levels ~ 1-2% of seawater. Human consumption of this fresh water source is exceeding recharge and lowering the groundwater table [51].

The structure of the Liwa Oasis interdune salt flats are inverted compared to most salt flats. In most locations with layers of saturated salt a continuing inflow from rain or tides brings a surface flow of relatively low salinity water, typically fresh water or seawater, onto the top of the salt-saturated layers. Thus, the salinity generally increases downward from either fresh or seawater at the surface to saturated salt at the bottom. The Liwa sabkha are unusual in that the surface is a thin layer of saturated salt and the relatively fresh water is flowing in from below the surface. The ground water level throughout the area of the sabkha is at, or just below, the surface. The future lowering of the level of the fresh ground water will alter the nature of the interdune sabkha communities. At the present time, the ground water reaches the surface of the sabhka site we studied and thus, just a few tens of cm below the salt flat surface, is relatively fresh water. This pattern, which is inverted compared to most other salt flats, is due to the thin translucent salt

117 crust surface, the upward flow of fresh water at the site and the lack of surface water flow in the
118 desert environment.
119
120 In this paper we report on studies of the physical and microbiological composition of the
121 inverted salt flat community in a Liwa Oasis sabkha. The interaction between the salt flat and the
122 ground water provides a sheltered habitat for microbial life in the desert. We document the
123 spatial distribution and identity of the organisms that live in this salinity and light gradient based
124 on 16S ribosomal RNA (rRNA) gene sequences as well as the sequences of the *mcrA* (methyl
125 coenzyme-M reductase) gene, which is present only in methane-producing microorganisms.
126 Microbial communities surviving in other arid environments, predominantly hypersaline
127 microbial mats, are known to contain methanogens, and to produce methane [6, 20, 29, 42]. This
128 is of interest both because methane is an important greenhouse gas in Earth's atmosphere and
129 because of the possible *in situ* detection of Martian methane by the Curiosity rover on Mars [45].
130
131 **Materials and Methods**
132
133 Study Site
134 The field studies did not involve endangered or protected species. A permit to conduct research
135 in the United Arab Emirates was obtained through the University of UAE via our co-author A.A.
136 Figure 1 shows the location of the Liwa Oasis and the extent of the hyper-arid zone in
137 southwestern UAE. The study site is located at N23.05088º E053.77005º at an elevation of 86 m.
138 Figure 3 shows a satellite image of the sabkha investigated here (dark area in the left part of
139 figure) and another nearby interdune flat area east of the study site. Interestingly, the surface of
140 the interdune flat area in the eastern site was not buried with sand in earlier online images (2009-
141 2010) but was buried on the date of our field work (February 2011) and is buried in images from
142 2014 onward as well.
143
144 At the study site there is a salt crust on the surface. This is seen in the foreground image in
145 Figure 4. The crust is compacted and can easily support pedestrian and vehicular traffic. Our
146 sample of the crust/endoevaportic mat is shown in Figure 5. Breaking the crust reveals wet
147 sediments below the surface crust layer. This is shown in the insert image in Figure 4 and the
148 overall vertical structure of the system is shown schematically in Figure 6. Endoevaporitic mats,
149 water and gas samples were gathered at two nearby locations in the sabkha.
150
151 Biological Samples
152 Endoevaporite mats were gathered by breaking away pieces from the overlying crust (as seen in
153 the insert in Figure 4). The mat shown in Figure 5 was brought back moist to NASA Ames
154 Research Center and sectioned at different depths based on the colored layers and then frozen at -
155 80ºC for later extraction and sequencing to characterize the bacterial community in each layer.
156
157 Water Samples
158 Water samples were collected from underneath the crust into sterile 50 ml conical tubes. pH was
159 measured on site using a photometer (Lovibond, CheckDirect, UK) and phenol red tablets.
160 Salinity was measured using a refractometer.
161
162 Gas Samples

163 Gas samples were collected from the same volume of material as the water samples, down to 20
164 cm, below the mats in the shallow sabkha water pools by prodding with a metal rod. Gas bubbles
165 produced by this disturbance were captured by water displacement in an inverted funnel fitted
166 with a syringe seal held over the area of sediments being disturbed. A syringe needle was
167 inserted through the seal, and the captured gas in the funnel was removed and re-injected into
168 evacuated serum bottles. Three gas samples were collected at each of the two shallow pools.

170 Methane (CH_4), carbon dioxide (CO_2), oxygen (O_2) and nitrogen (N_2) concentrations were
171 determined at NASA Ames Research Center using a Shimadzu 14A gas chromatograph (GC).
172 Methane concentrations were measured with a flame ionization detector fitted with a Porapak N
173 column, with N_2 as the carrier gas. CO_2 was measured using a thermal conductivity detector
174 (TCD) fitted with a Porapak N column with helium as the carrier gas. N_2 and O_2 were analyzed
175 using a TCD fitted with a molecular sieve packed column, with helium as the carrier gas.
176 Matheson Tri-gas 100 ppm CH_4, 20% O_2/79% N_2, and 1% CO_2 standards were run along with
177 samples.

179 Gas samples for stable carbon isotopic analysis of methane were processed at Florida State
180 University. Methane concentrations were determined using a Shimadzu Mini-2 gas
181 chromatograph (GC) with a flame-ionization detector, fitted with a 1.83-m, 1/8in. (3.1 mm)
182 stainless steel tubing packed with HayeSep Q 80/100 mesh. All samples were handled by
183 directly injecting the gas (~250 μL) into the GC, where the sample was carried by UHP helium
184 for analysis. Multiple methane standards (Scott Gas, PA, USA) were run along with samples.
185 The analytical errors for methane concentration analyses are ±0.5 ppm. Stable carbon isotope
186 values were obtained using a modified cryofocusing method to amplify the methane peak [34,
187 42]. Isotope analyses were performed using the methods described in detail in Tazaz et al. [42]
188 and are only briefly summarized here. Duplicate analyses were performed on all gas samples.
189 Carbon isotope data are reported in the ''del'' notation (e.g., $\delta^{13}C$) [42]:

191 $\delta^{13}C = 1000[^{13}C/^{12}C \text{ sam}/ ^{13}C/^{12}C \text{ std} - 1]$,

193 where sam refers to the sample and std to the standard, Pee Dee belemnite (PDB). The units of δ
194 are permil (‰). The analytical errors for stable isotopic analyses are ±0.4‰ for $\delta^{13}C$ in methane.

196 Nucleic Acid extractions
197 Genomic DNA was extracted from each layer of the mat, hereafter referred as top, middle,
198 bottom and sediment layers (Figure 5), in triplicate using the MO BIO Power Biofilm DNA
199 isolation kit (#24000-50; MO BIO Laboratories, Inc., Carlsbad, CA, USA) and a bead beater to
200 lyse the cells according to the product manual. The extracted DNA was analyzed on an agarose
201 gel to assess the quality of the extractions, and quantified on a spectrophotometer (P330
202 nanophotometer; Implen Inc., Westlake Village, CA, USA).

204 PCR amplification
205 Bacterial 16S rRNA genes for all DNA extractions were amplified using the universal primers
206 8F (5' -AGAGTTTGATCCTGGCTCAG -3') and 1492R (5' -GGTTACCTTGTTACGACTT-
207 3') [23,43]. Triplicate PCR reactions were run for each sample, with each PCR mixture
208 containing 0.6 μl of each primer (50 μM), 12.5 μl of GoTaq Green master mix (M7122;

209 Promega, Madison, WI, USA), 1 μl of DNA template (~20 ng/μl) and 10.3 μl of nuclease-free
210 water for a maximum reaction volume of 25 μl. The 16S rRNA PCR program was set to: 95°C
211 for 10 min, followed by 28 cycles each at 95°C for 0.5 min, 55°C for 1 min, 72°C for 1.5 min,
212 ending with one final extension cycle at 72°C for 12 min in a Peltier thermocycler PTC-200 (MJ
213 Research Inc., Waltham, MA, USA). The *mcrA* gene was amplified using the *mcrA* primers
214 described in Luton et al [25]. Triplicate PCR reactions were run for each sample, with each PCR
215 mixture containing 1 μl of each primer (10 μM), 12.5 μl of GoTaq Green master mix (M7122;
216 Promega, Madison, WI, USA), 1 μl of DNA template (~20 ng/μl) and 9.5 μl of nuclease-free
217 water for a maximum reaction volume of 25 μl, using the following PCR program: 95°C for 1
218 min, 35 cycles at 94°C for 30 s, 55°C for 30 s, 72°C for 1 min with a final extension cycle at
219 72°C for 5 min according to Garcia-Maldonado et al. 2014 [18]. A second amplification was
220 performed for 25 cycles using 2 μl of *mcrA* PCR product from the first amplification to get more
221 distinct bands. All amplifications were analyzed along with positive and negative controls for
222 quality control.
223
224 Replicate PCR products were pooled and run on an agarose gel for each gene. The 16S rRNA
225 and *mcrA* fragments were excised and purified using the Omega E.Z.N.A. gel extraction kit
226 (D2500-01; Omega Bio-Tek Inc., Norcross, GA, USA) according to manufacturer instructions.
227 Prior to cloning, a poly(A) tail reaction was performed on all 16S rRNA samples by adding 6 μl
228 of PCR product, 1 μl 10X PCR buffer, 1 μl MgCl$_2$, 1 μl dNTP, and 1 μl Taq polymerase to a
229 total volume of 10 μl per sample and heating the samples to 72°C for 20 min in a thermo cycler.
230
231 Cloning
232 The Life Technologies TOPO TA Cloning Kit for Sequencing (#K457501) (Life Technologies,
233 Carlsbad, CA, USA) was used to ligate 4 μl of the purified PCR product to 1 μl of cloning vector
234 (pCR4-TOPO) in addition to 1 μl of salt solution, followed by the vector-PCR insertion into One
235 Shot Top10 Chemically Competent *E. coli* cells according to the product manual. The cells were
236 plated at different densities on Luria Broth (LB) agar plates containing 50 μg/μl of ampicillin,
237 0.2 mM IPTG and 40 μg/ml X-gal, and were incubated at 37°C overnight. For each layer, white
238 colonies were picked and transferred to individual wells in a deep 96-well plate containing 500
239 μl of LB medium, 10% glycerol and 100 μg/ml ampicillin, and were grown overnight at 37°C.
240 Ninety-six clones per layer were shipped in dry ice to Beckman Coulter Genomics (Danvers,
241 MA, USA) for Sanger sequencing of the 16S rRNA gene on an ABI PRISM 3730xl DNA
242 analyzer (Applied Biosystems, Foster City, CA, USA). Clones with the *mcrA* gene insert were
243 verified by PCR using plasmid specific M13 primers, purified using the PureLink Quick
244 Plasmid Miniprep kit (#K210010) (Life Technologies, Carlsbad, CA) and submitted to ELIM
245 Biopharmaceuticals, Inc. (Hayward, CA, USA) for Sanger sequencing on an ABI PRISM 3720xl
246 DNA analyzer.
247
248 Nucleotide sequence data and classification
249 Full length Sanger reads were obtained through Beckman Coulter Genomics single pass standard
250 sequencing read service using the primers T3 (5' -ATTAACCCTCACTAAAGGGA- 3'), T7 (5'
251 -TAATACGACTCACTATAGGG- 3') and 515 (5' -GTGCCAGCAGCCGCGGTAA- 3') for the
252 16S sequences. The three reads per sample were quality-filtered, trimmed and assembled to full
253 16S sequences (~1.5 kb) using the software Geneious (V. 7.1.6; Biomatters Ltd., Auckland, NZ).
254 Assemblies containing less than 3 reads were discarded. Full 16S sequences were aligned with

255 the *E. coli* strain K-12 (U00096) as a reference using the SILVA Incremental Aligner (SINA)
256 (v1.2.11) program provided by the SILVA ribosomal RNA project; http://www.arb-
257 silva.de/aligner/) as described in Pruesse et al. [33]. Columns in the alignments with common
258 gaps were removed using the filter.seqs command in the open-source software MOTHUR
259 (http://www.mothur.org/) [38]. Chimeras were identified using the software Mallard (v. 1.02)
260 with a cut-off line set to 99.9%, as described in Ashelford et al. [4]. The nucleotide sequence of
261 outliers (samples with deviation from expectation (DE) values above the set cut-off line in
262 Mallard) were queried manually against the NCBI non-redundant nucleotide sequence database
263 using the BLASTN program (http://blast.ncbi.nlm.nih.gov/Blast.cgi) [56] to further assess if
264 these were real chimeras, and were discarded if chimeric breakpoints in sequences were evident
265 in BLAST results. After quality control, we ended with a total of 317 16S sequences, with 71,76,
266 85 ,85 for the top, middle, bottom and sediment layer, respectively. Single pass standard
267 sequencing reads for *mcrA* using the M13 F primer were obtained through ELIM
268 Biopharmaceuticals, Inc. Sequences were quality filtered and manually trimmed using
269 CodonCode Aligner (v4.0.4; CodonCode Corp., Centerville, MA) and aligned using Clustal X
270 2.1 [23], a function in the software MEGA 6 [22].
271
272 The search and classify tool in SINA was used for taxonomic assignment of the 16S sequences
273 based on the last common ancestor method. Representative sequences for each phylum were
274 further queried against the NCBI nucleotide database using the BLASTN program. Sequences
275 identified as belonging to the genus *Salinibacter* were further analyzed in MOTHUR [38]. The
276 cluster command was used to identify operational taxonomic units (OTUs) with a 0.01 cutoff
277 using the average neighbor algorithm.
278
279 All sequences determined in this study were deposited in the NCBI database under GenBank
280 accession numbers KU308828 - KU309144 for 16S rRNA sequences, and KU514395-
281 KU514406 for *mcrA* sequences.
282
283 **Results**
284 Water collected from the two sampling pools (Figure 4 insert) was measured for salinity and pH.
285 Gases collected as bubbles were analyzed for O_2, N_2, CO_2 and CH_4 content and $^{13}C/^{12}C$ isotope
286 values. Water in the shallow pools was uniformly 30ºC at the time of measurement. The results
287 are shown in Table 1 as the average and standard deviation of three replicate samples at two
288 nearby sites. Although the two samples only differ only slightly in salinity, the oxygen levels
289 differ by a factor of ~ 2, but with large variation between replicates. Methane concentration is
290 high in both samples indicating a source of methane in the salt flat. Carbon dioxide and methane
291 are distinct between the two samples (no overlap of the error bars) and they co-vary.
292
293 The presence of methanogenic microorganisms at this site was confirmed through the
294 amplification of the *mcrA* gene (~470 bp) from the bottom and sediment layers; the gene was
295 not amplified from the top and middle layers. Twelve sequences obtained from these samples
296 yielded close matches (>91% nucleotide identity scores) to methanogenic archaea: the extremely
297 halophilic *Methanohalobium evestigatum* (CP002069) [57], the moderately halophilic
298 *Methanolobus vulcani* (U22245) and *Methanohalophilus portucalensis* (AB908273) [3,48] based
299 on BLAST analysis.
300

Further microbial community composition analysis of the salt crust revealed the presence of a
diverse microbial community with unusual layering with primary productivity based on
photosynthesis. Based on the distribution of identified environmental sequences, the top and
middle layers of the endovaporitic mat were dominated by the phylum *Bacteroidetes* (~63.4%),
with a gradual decrease in abundance with increasing depth (Figure 7). Sequences most similar
to those from the genus *Salinibacter*, an extreme halophile that thrives at salinity levels of 20-
30% [28], was the dominant representative in the top three layers. Sequences for mild to
moderate halophiles of the genera *Gracilimonas*, *Marivirga* (0.5-10%) and *Owenweeksia* (1-
7.5%) were only identified in the sediment layer (Table 2) [32,35,44]. In contrast, cyanobacterial
sequences were only found in low abundances in the top and middle layers (2.8% and 5.3%,
respectively), and higher abundance in the bottom and sediment layers at 42.4 and 33%,
respectively (Figure 7). Representative cyanobacterial sequences identified were most similar to
the unicellular, halotolerant, coccoid *Cyanothece* sp., *Euhalothece* sp. and *Dactylococcopsis
salina*. The taxonomic distribution of members of the *Bacteroidetes* and *Cyanobacteria* phyla
along the vertical profile are consistent with the presence of a salinity gradient in this sabkha,
where the top layer of the endoevaporitic mat has a high salinity, and the lower layer is
influenced by a lower salinity due to the presence of fresh groundwater. Sequences from the
phylum *Proteobacteria* were present in all four layers, but were almost twice as abundant in the
sediment layer, which was mostly composed of fine sand. Based on genus-level identities
provided by the SINA analysis, this phylum was the most diverse in our clone libraries in terms
of richness. Within these sequences, representatives of the *Alphaproteobacteria*,
Gammaproteobacteria, and *Deltaproteobacteria* classes were identified (Table 2). Sequences
with low-identity to the *Gemmatimonadetes* and sequences most similar to *Verrucomicrobia*
were less common and only present in the lower two layers. Sequences with unknown identity
were categorized as "other" and varied from 2.8 to 8.2% in abundance of total sequences.

Plastid sequences belonging to phototrophic eukaryotes were also identified and placed in a
"plastids" category. These were present in the top (14.1%), middle (5.3%) and bottom (4.7%)
layers (Figure 7). The closest identities to these plastids were for the unicellular, flagellated
marine Chlorophytes *Dunaliella tertiolecta* and *Crustomastix stigmatica* (Table 2). *Dunaliella*
was also observed through light microscopy in fresh mat samples. Due to their motility via
flagella, these phototrophic eukaryotes may not only be able to move between layers, but also
populate the water below the endoevaporitic crusts.

After additional curation to remove shorter sequences, 110 of the clones identified by SINA as
most similar to *Salinibacter* were further examined using an OTU-based approach. For the top,
middle, bottom, and sediment samples, there were 40, 45, 22 and 3 *Salinibacter* sequences,
respectively. At 0.01 cutoff (99% similarity), 11 distinct OTUs were identified (Table 3). The
largest OTU contained 62 sequences (56.4%), and four OTUs contained only a single sequence.
Although the present survey only allows for qualitative comparisons of the depth distribution of
these OTUs, there appeared to be a by-sampling partition for OTUs 1, 2 and 5 (mainly in the top
and middle samples), and OTUs 3 and 4 (mainly found in the bottom sample). OTU 6 appeared
to be cosmopolitan with representation in all samples, but with only 5 sequences total, this is not
definitive (Table 3). A phylogenetic analysis of representative sequences from the OTUs with
multiple sequences supported the use of a 0.01 cutoff for the clustering, but did not reveal any
divergence patterns consistent with the location of the OTU within the sabkha (not shown).

Discussion

From the physical setting of the salt flat we expect that light levels and salinity should systematically decrease with depth. The case of oxygen is more complex, the deep ground water contains oxygen, and oxygen is present in the atmosphere at the surface. However microbial processes in the mat consume oxygen and can produce anoxic layers. Hence while oxygen levels may decrease with depth from the surface, layers deep enough to be in the unaltered groundwater will have high oxygen content. The two salty samples (320 and 340 ppt) in Table 1 represent shallow subsurface solutions that have interacted with the salt crust and have been exposed to some extent to the ambient atmosphere. The high methane and carbon dioxide levels argue against the oxygen being preserved from the ground water; there is no evidence of vigorous mixing of ground water with material in the biological layers.

The sampling method was inadequate to directly characterize the salinity profile below the salt crust with depth in a systematic way and we make no attempt to assign a depth difference to these samples. Nor can we exclude the possibility that our samples represent material from a range of depths mixed together by the creation of the sampling pond which would imply that the differences in salinity and oxygen are not significant. The salinity in both sampling pools indicated nearly saturated conditions (solubility of NaCl in water at 30°C is 360 ppt). In contrast, groundwater that had been pumped into a nearby holding tank for irrigation use had a salinity of 17 ppt in agreement with published data [51] indicating, as mentioned above, the groundwater has low salinity.

The methane content differs between the two samples, increasing to 3442 ppm for the lower salinity, lower oxygen, higher carbon dioxide sample. It seems plausible that methane content would be higher in the lower salinity layers with lower oxygen levels. However, we note that we cannot rule out migration of methane gas through the system against, or with, the flow of water. Clearly further measurements are required to understand the depth profile.

The presence of methanogens at this site was strongly suggested by the amplification of the *mcrA* gene, unique to methanogens, from the bottom two layers of the mat and high sequence identities to three phylogenetic groups of methanogenic archaea. The presence of methanogens was also confirmed by the detection of methane (0.3% v/v) in bubbles collected from this site, with δ^{13}C values comparable to those reported in endoevaporitic mats [20,21,42]. The unusually enriched δ^{13}C values (-41‰ and -38‰) are higher than the traditional δ^{13}C values expected for biogenic methane (~<-50‰) [21,39,42,46], but may be explained by lower isotopic fractionation in systems where substrate is limited, such as in high-salinity endoevaporitic mats [20,21,42]. Methane oxidation may also result in more enriched δ^{13}C values, but methanotrophs are thought to be mostly absent in hypersaline environments [8]. However, our 16S sequences did include one representative with similarity to the methanotrophic *Methylohalomonas lacus* in the sediment layer (Table 2).

The significance of the methane is twofold. First it represents a source of methane in a desert environment on Earth contributing to the global inventory of methane sources. Secondly

392 methane production in this sabkha provides one possible model for methane production on Mars,
393 as discussed below.
394
395 Studies of orbital images over the past 40 years show no detectable change in the position of the
396 dunes or the location of the sabkhas. This indicates that the timescale for covering and
397 uncovering new sabhka flats is in excess of hundreds of years. Based on satellite images and
398 GPS ground observations over several years, Lorenz and Radebaugh [24] computed a net motion
399 of ~0.1 m/yr advance for the large dunes of the Liwa Oasis. The sabhka studied here was about
400 500 m in diameter (Figure 2) suggesting a lifetime against burial by the large dunes of 5000
401 years. It may be possible to discover previously buried sabkha in this area exposed by recent
402 movement of the dunes and thus investigate the preserved remains of past mat systems.
403
404 An important contrast between this environment and previous studies of salt ponds and coastal
405 sabkhas is the salinity gradient. In most hypersaline environments in deserts or coastal sites the
406 salt arrives with the water supply from above the surface and accumulates as the water
407 evaporates. In the Liwa Oasis sabkha studied here, the water flow is in the subsurface; there is
408 very little surface flow. This creates an unusual layered structure with saturated salt layers on top
409 and relatively freshwater layers below. The structure of the microbial mat (Figure 5) is the
410 clearest indication we have of this vertical structuring due to light, salinity and oxygen gradients.
411 Clone libraries constructed from four depths within the sabkha crust showed changes in
412 taxonomic composition consistent with decreasing salinity with depth (e.g., reduced total and
413 proportional abundances of *Salinibacter* sequences), but further research is required to
414 understand the role this gradient has on structuring the microbial community. This gradient is
415 shown schematically in Figure 6.
416
417 The interdune sabkhas in Liwa Oasis are of particular interest as a Mars analog. The salt crust is
418 a relic deposited by previous evaporation. Although widespread, the salt crust is not easily
419 visible by remote sensing because it is mixed in with sand. Similar relic salt flats may exist on
420 Mars today, remnants from a wetter period in the past buried by the present shifting sands. The
421 sabkha studied here suggests an alternative way these salt deposits could support life. If there
422 was a source of deep ground water flowing upward from below, a near-surface habitable layer
423 might be formed protected from the low pressure, arid surface conditions. The results from the
424 Liwa Oasis suggest a microbial model for such a habitat and for methane production at such a
425 site. Light can penetrate the salt crust providing energy for photosynthesis but provides a barrier
426 to loss of water into the dry atmosphere due both to physically blocking exchange between the
427 water and the atmosphere and by lowering the vapor pressure of water due to solution. This
428 reduction of water loss by the salt layer operates in the Liwa Oasis as it would on Mars.
429
430 In the Liwa Oasis, methane is being released from the salt community continuously as the salt
431 pan is fractured in many places. This would not be the case on Mars as the pan would have to be
432 tightly sealed to preserve the liquid water habitat below. On Mars methane would build up below
433 the salt pan until the gas pressure exceeded the pressure holding the salt pan down, the vapor
434 pressure of water, assuming it is cold, would barely exceed the ambient pressure and hence alone
435 would not suffice to break the surface. The pan would then crack with a sudden release of gas.
436 Rapid evaporation and flash freezing of the outflowing water on the surface would quickly reseal
437 the crack with ice, which would slowly sublime leaving behind sediment and salt. The cycle

might repeat on timescale of years or even decades. Such a system could conceivably explain large outbursts of methane on Mars as has been reported [26]. However it does not provide an explanation for the subsequent rapid loss of the methane plumes also reported [26]. This rapid loss is inconsistent with known photochemical processes on Mars [55].

A salt pan system such as studied here can prolong habitability for photosynthetic surface biology when only ground water is available and surface conditions are unsuitable for stable liquid water. Another important aspect of this system is the preservation of biomarkers, including methane and other evidence for life in the salt after it dries out. Such a near surface system could be accessed by surface rovers. If an inverted salt mat system fed by groundwater existed on Mars in the past but is no longer operative it may still be of considerable astrobiology interest. It has been suggested [36] that salt deposits can preserve evidence of past life. As the flow of water to the inverted mat ceased, the active microbial system would be encased in salt and preserved over geological time, relatively protected from radiation and oxidation damage.

Acknowledgements

References

1. Al-Farraj A (2005) An evolutionary model for sabkha development on the north coast of the UAE. J Arid Environ 63: 740-55.
2. Al-Katheeri ES Howari FM Murad AA (2009) Hydrogeochemistry and pollution assessment of quaternary–tertiary aquifer in the Liwa area United Arab Emirates Environmental Earth Sciences 59: 581-592.
3. Antony CP Murrell JC Shouche YS (2012). Molecular diversity of methanogens and identification of Methanolobus sp. as active methylotrophic Archaea in Lonar crater lake sediments. FEMS microbiology ecology 81(1): 43-51.
4. Ashelford KE Chuzhanova NA Fry JC Jones AJ Weightman AJ (2006) New screening software shows that most recent large 16S rRNA gene clone libraries contain chimeras. App Environ Microbio 72: 5734-5741.
5. Barbieri R Stivaletta N Marinangeli L Ori GG (2006) Microbial signatures in sabkha evaporite deposits of Chott el Gharsa (Tunisia) and their astrobiological implications. Plt. Space Sci 54: 726-36.
6. Bebout BM Hoehler TM Thamdrup B Albert D Carpenter SP Hogan M Turk K Des Marais DJ (2004) Methane production by microbial mats under low sulphate concentrations. Geobiology 2: 87-96.
7. Böer B (1997) An introduction to the climate of the United Arab Emirates. J Arid Environ 35:3-16.

483   8. Conrad R., P. Frenzel, Y. Cohen. 1995. Methane emission from hypersaline microbial mats:
484   Lack of aerobic methane oxidation activity. FEMS Microbiol. Ecol. 16: 297-306.

485   9. Davila AF Duport LG Melchiorri R Janchen J Valea S de Los Rios A Fairén AG 1Diedrich
486   Möhlmann D McKay CP Ascaso C Wierzchos J (2010) Hygroscopic salts and the potential
487   for life on Mars. Astrobiology 10: 617-628.

488 10. Davila AF Gross C Marzo GA Fairén AG Kneissl T McKay CP Dohm JM (2011) A large
489   sedimentary basin in the Terra Sirenum region of the southern highlands of Mars. Icarus 212:
490   579-589.

491 11. Douglas S (2004) Microbial biosignatures in evaporite deposits: Evidence from Death
492   Valley, California. Plt. Space Sci 52: 223-227.

493 12. Douglas S Yang H (2002) Mineral biosignatures in evaporites: Presence of rosickyite in an
494   endoevaporitic microbial community from Death Valley, California. Geology 30: 1075-1078.

495 13. Douglas S Abbey W Mielke R Conrad P Kanik I (2008) Textural and mineralogical
496   biosignatures in an unusual microbialite from Death Valley, California. Icarus 193: 620-636.

497 14. Edwards HM Mohsin M Sadooni F Nik Hassan N Munshi T. Life in the sabkha: Raman
498   spectroscopy of halotrophic extremophiles of relevance to planetary exploration. Anal
499   Bioanal Chem 385: 46-56.

500 15. El-Sayed MI (1999) Sedimentological characteristics and morphology of the aeolian sand
501   dunes in the eastern part of the UAE a case study from Ar Rub' Al Khali. Sediment Geol 123:
502   219-238.

503 16. El-Sayed MI (2000) The nature and possible origin of mega-dunes in Liwa Ar Rub' Al Khali
504   UAE. Sediment Geol 134: 305-330.

505 17. Evans G (1970) Coastal and nearshore sedimentation: A comparison of clastic and carbonate
506   deposition. Proceedings of the Geologists' Association 81: 493-508.

507 18. Garcia-Maldonado JQ Bebout BM Everroad RC López-Cortés A (2014) Evidence of novel
508   phylogenetic lineages of methanogenic archaea from hypersaline microbial mats. Microbial
509   Ecology 69:106-117.

510 19. Glennie KW (1998) The desert of southeast Arabia: a product of Quaternary climate change
511   In: Alsharhan A Glennie K Whittle G Kendall C (Eds.) Quaternary Deserts and Climatic
512   Change Balkema Rotterdam pp 279 – 291.

513 20. Kelley CA Poole JA Tazaz AM Chanton JP Bebout BM (2012) Substrate limitation for
514   methanogenesis in hypersaline environments. Astrobiology 12:89 –97.

515 21. Kelley CA Nicholson BE Beaudoin CS Detweiler AM Bebout BM (2014). Trimethylamine
516   and organic matter additions reverse substrate limitation effects on the δ13C values of
517   methane produced in hypersaline microbial mats. Applied and Environmental Microbiology
518   80: 7316-7323.

519 22. Lane DJ (1991) 16S/23S rRNA sequencing. In: Nucleic acid techniques in bacterial
520   systematics. Stackebrandt E. and Goodfellow M. eds. John Wiley and Sons, New York, NY,
521   pp. 115-175.

522 23. Larkin MA Blackshields G Brown NP Chenna R McGettigan PA McWilliam H Valentin F
523   Wallace IM Wilm A Lopez R Thompson JD Gibson TJ Higgins DG (2007) Clustal W and
524   Clustal X version 2.0. Bioinformatics 23(21):2947-2948.

525 24. Lorenz RD Radebaugh J (2015) Giant Linear Dunes as the Formation Pathway to
526   Megabarchan Chains : Titan and the Rub 'Al Khali. Fourth International Planetary Dunes
527   Workshop (2015) abstract 8003.

528 25. Luton PE Wayne JM Sharp RJ Riley PW (2002) The *mcrA* gene as an alternative to 16S
529   rRNA in the phylogenetic analysis of methanogen populations in landfill. Microbiology
530   148:3521-3530.
531 26. Mumma MJ Villanueva GL Novak RE Hewagama T Bonev BP. DiSanti MA. Mandell AM
532   Smith MD (2009) Strong release of methane on Mars in northern summer 2003. Science,
533   323(5917): 1041-1045.
534 27. Ojha L Wilhelm MB Murchie SL McEwen AS Wray JJ Hanley J Massé M Chojnacki M
535   (2015) Spectral evidence for hydrated salts in recurring slope lineae on Mars. Nature
536   Geoscience 8(11): 829-832.
537 28. Oren A (1988) Anaerobic degradation of organic compounds at high salt concentrations
538   Antonie van Leeuwenhoek 54: 267-277.
539 29. Oren A (2013) Salinibacter: an extremely halophilic bacterium with archaeal properties
540   FEMS Microbiol Lett 342: 1-9.
541 30. Osterloo MM Hamilton VE Bandfield JL Glotch TD Baldridge AM Christensen PR
542   Tornabene LL Anderson FS (2008) Chloride-bearing materials in the southern highlands of
543   Mars. Science 319: 1651-1654.
544 31. Osterloo MM Anderson FS Hamilton VE Hynek BM (2010) Geologic context of proposed
545   chloride-bearing materials on Mars. J Geophys Res 115 E10012
546 32. Pagani I Chertkov O Lapidus A Lucas S Del Rio TG Tice H et al. (2011) Complete genome
547   sequence of *Marivirga tractuosa* type strain (H-43). *Standards in Genomic Sciences*, *4*(2),
548   154–162. doi:10.4056/sigs.1623941
549 33. Pruesse E Peplies J Glockner FO (2012) SINA: accurate high-throughput multiple sequence
550   alignment of ribosomal RNA genes. Bioinformatics 28: 1823-1829.
551 34. Rice AL Gotoh AA Ajie HO Tyler SC (2001). High-precision continuous-flow measurement
552   of δ13C and δD of atmospheric CH4. Analytical Chemistry 73: 4104-4110.
553 35. Riedel T Held B Nolan M Lucas S Lapidus A Tice H. et al. (2012). Genome sequence of the
554   orange-pigmented seawater bacterium *Owenweeksia hongkongensis* type strain
555   (UST20020801[T]). *Standards in Genomic Sciences*, *7*(1), 120–130. doi:10.4056/sigs.3296896
556 36. Rothschild LJ (1990) Earth analogs for Martian life. Microbes in evaporites a new model
557   system for life on Mars Icarus 88: 246-60.
558 37. Rothschild LJ Giver LJ White MR Mancinelli RL (1994) Metabolic activity of
559   microorganisms in evaporates. J Phycol 30: 431-438.
560 38. Schloss PD Westcott SL Ryabin T Hall JR Hartmann M Hollister EB et al (2009)
561   Introducing mothur: open-source, platform-independent, community-supported software for
562   describing and comparing microbial communities. Appl Environ Microbiol 75: 7537-7541.
563 39. Sherwood-Lollar B Lacrampe-Couloume G Slater GF Ward J Moser DP Gihring TM Lin L-
564   H Onstott TC (2006) Unravelling abiogenic and biogenic sources of methane in the Earth's
565   deep subsurface. Chemical Geology 226: 328-339.
566 40. Shinn EA Robbin DM (1983) Mechanical and chemical compaction in fine-grained shallow-
567   water limestones. Journal of Sedimentary Research 53 no 2.
568 41. Tamura K Stecher G Peterson D Filipski A Kumar S (2013). MEGA6: molecular
569   evolutionary genetics analysis version 6.0. Molecular biology and evolution, 30(12): 2725-
570   2729.
571 42. Tazaz AM Bebout BM Kelley CA Poole J Chanton JP (2013) Redefining the isotopic
572   boundaries of biogenic methane: Methane from endoevaporites. Icarus 224: 268-275.

573 43. Turner S. Pryer K.M. Miao V.P.W. and Palmer J.D. 1999. Investigating deep phylogenetic
574   relationships among cyanobacteria and plastids by small subunit rRNA sequence analysis.
575   Journal of Eukaryotic Microbiology 46: 327–338.
576 44. Wang YX Li YP Liu JH Xiao W Lai YH Li ZY Ding ZG Wen ML Cui XL (2013)
577   Gracilimonas mengyeensis sp. nov., a moderately halophilic bacterium isolated from a salt
578   mine in Yunnan, south-western China. Int. J. Syst. Evol. Microbiol., 63, 3989-3993. doi:
579   10.1099/ijs.0.052043-0.
580 45. Webster CR et al. (2015) Mars methane detection and variability at Gale crater. Science 347:
581   415-417.
582 46. Whiticar MJ (1999) Carbon and hydrogen isotope systematics of bacterial formation and
583   oxidation of methane Chemical Geology 161: 291-314.
584 47. Wierzchos J Ascaso C McKay CP (2006) Endolithic cyanobacteria in halite rocks from the
585   hyperarid core of the Atacama Desert Astrobiology 6: 415-422.
586 48. Wilharm, T., Zhilina, T. N., & Hummel, P. (1991). DNA-DNA Hybridization of
587   Methylotrophic Halophilic Methanogenic Bacteria and Transfer of Methanococcus
588   halophilusvp to the Genus Methanohalophilus as Methanohalophilus halophilus comb. nov.
589   International journal of systematic bacteriology, 41(4), 558-562.
590 49. Wood WW (2011). Source of paleo-groundwater in the Emirate of Abu Dhabi, United Arab
591   Emirates: evidence from unusual oxygen and deuterium isotope data. *Hydrogeology journal*,
592   *19*(1), 155-161.
593 50. Wood WW Imes JL (1995) How wet is wet? Constraints on late Quaternary climate in the
594   southern Arabian Peninsula. J Hydrol 164:263–268
595 51. Wood WW Imes JL (2003) Dating of Holocene Ground-water recharge in western part of
596   Abu Dhabi (United Arab Emirates): Constraints on global climate-change models.
597   Developments in Water Science 50: 379-385.
598 52. Wood WW Sanford WE Al Habschi ARS (2002) The source of solutes in the coastal sabkha
599   of Abu Dhabi. Bull Geol Soc Am 114:259–268.
600 53. Wood WW Rizk ZS Alsharhan AS (2003). Timing of recharge, and the origin, evolution and
601   distribution of solutes in a hyperarid aquifer system. *Developments in water science*, *50*, 295-
602   312.
603 54. Wood WW Rizk ZS Alsharhan AS (2003) Timing of recharge, and the origin, evolution, and
604   distribution of solutes in a hyperarid aquifer system, in water resources perspectives:
605   evaluation, management and policy. In: Alsharhan AS, Wood WW (eds) Developments in
606   water science, vol 50. Elsevier, Amsterdam, pp 295–312
607 55. Zahnle K Freedman RS Catling DC (2011) Is there methane on Mars? Icarus 212: 493-503.
608 56. Zhang Z Schwartz S Wagner L Miller W (2000) A greedy algorithm for aligning DNA
609   sequences. J Comput Bio 7: 203-214.
610 57. Zhilina TN Zavarzin GA (1987) *Methanohalobium evestigatu*m gen. nov., sp. nov.,
611   extremely halophilic methane producing archaebacteria. Dokl. Akad. Nauk. SSSR 239:464-
612   468.
613

614

615 Table 1. Salinity and pH of water samples, and gas composition of released bubbles from the sabkha
616 subsurface.

Salinity, ppt	CH_4, ppm	$\delta^{13}CH_4$, ‰	pH	CO_2, %	O_2, %	N_2, %
320	3442±343	-38.46 ±1.25	7.67	0.65±0.02	0.96±0.07	97.45±0.40
340	2257±154	-41.14 ± 0.27	7.67	0.22±0.05	1.73±0.98	96.61±1.07

617
618

Table 2. Select identities of closest cultured matches based on longest sequences for the phyla identified in each layer, using the NCBI BLASTN program. Proteobacteria representatives are additionally identified as belonging to the class *Alphaproteobacteria* (A), *Deltaproteobacteria* (D), or *Gammaproteobacteria* (G). The sequence similarity is indicated by ID% with similarities of 99% marked with bold type.

Layer	Phylum	Most related sequences	ID%	Accession #
Top				
	Bacteroidetes	*Salinibacter sp.*	97	AY987850
		Salinibacter luteus	**99**	NR_117935
		Salinibacter iranicus	**99**	NR_117934
	Proteobacteria	*Arhodomonas recens* (G)	95	NR_118045
		Thioalkalivibrio sulfidophilus (G)	92	NR_074692
		Limimonas halophila (A)	**99**	NR_109490
		Azospirillum sp. (A)	90	EU264075
		Erythrobacter litoralis (A)	98	NR_074349
	Cyanobacteria	*Cyanothece sp. 104*	**99**	DQ243687
	Plastids	*Dunaliella tertiolecta*	98	JQ039090
Middle				
	Bacteroidetes	*Salinibacter sp.*	98	AY987850
		Salinibacter iranicus	**99**	NR_117934
	Proteobacteria	*Thiohalorhabdus denitrificans* (G)	93	EU374712
		Arhodomonas recens (G)	94	NR_118045
		Proteobacterium FA350 (D)	87	KM034744
		Aquisalimonas sp. (G)	98	KC577145
		Limimonas halophila (A)	**99**	NR_109490
	Cyanobacteria	*Cyanothece sp. 115*	**99**	DQ243690
		Euhalothece sp.	97	AJ000710
	Plastids	*Crustomastix stigmatica*	84	FN563093
Bottom				
	Bacteroidetes	*Salinibacter ruber*	96	CP000159
		Salinibacter sp.	96	KF569484

Proteobacteria	*Limimonas halophila* (A)	**99**	NR_109490
	Arhodomonas recens (G)	94	NR_118045
	Proteobacterium FA350 (D)	85	KM034744
Cyanobacteria	*Euhalothece sp.*	96	AJ000713
Gemmatimonadetes	*Rubrobacter xylanophilus*	83	NR_074552
Plastids	*Crustomastix stigmatica*	84	FN563093
Sediment			
Bacteroidetes	*Salinibacter sp.*	96	KF569484
	Gracilimonas sp.	96	KJ206435
	Salinibacter ruber	95	AF323502
	Salinibacter iranicus	96	NR_117934
	Marivirga tractuosa	98	NR_074493
Proteobacteria	*Methylohalomonas lacus* (G)	95	NR_043973
	Halomonas gudaonensis (G)	**99**	NR_043807
	Thioalkalivibrio sulfidophilus (G)	91	NR_074692
	Halospina denitrificans (G)	97	NR_043525
	Erythrobacter litoralis (A)	98	NR_074349
	Aquisalimonas sp. (G)	**99**	KC577145
Cyanobacteria	*Cyanothece sp. 104*	**99**	DQ243687
	Euhalothece sp.	96	AJ000713
	Dactylococcopsis salina	**99**	NR_102465
Gemmatimonadetes	*Thermaerobacter marianensis*	83	CP002344
Verrucomicrobia	*Coraliomargarita akajimensis*	95	NR_074901

625

Table 3. Abundance and distribution of *Salinibacter* OTUs

OTU #	Number of clones				
	Top	Middle	Bottom	Sediment	Total
1	27	31	4	0	62
2	3	6	1	0	10
3	0	2	7	1	10
4	1	1	7	0	9
5	4	4	0	0	8
6	1	1	2	1	5
7	1	0	1	0	2
8	0	0	0	1	1
9	1	0	0	0	1
10	1	0	0	0	1
11	1	0	0	0	1
Total	40	45	22	3	110

628
629   Figure 1. Map adapted from Böer [7] showing the approximate field location (red dot) of the Liwa Oasis
630   Sabkhas explored in this study. White areas are hyper-arid, stippled grey areas are arid, dark areas are
631   semi-arid and grey areas are sub-humid. Very light grey is the Arabian Gulf. The UAE boader is shown as
632   a dotted line.

633
634   Figure 2. Schematic of the aquifer contained within the dunes of the Liwa Oasis. The base of the dunes is
635   a relatively impermeable layer of carbonate close to sea level (striped layer). The solid line represents the
636   dune profile, the dotted line the aquifer. Flow lines are indicated. Discharge occurs at the lower elevations
637   of the dune where the water table comes close to or intersects the surface. Evaporation occurs leaving
638   behind salt. In the flat interdune spaces salt flats (sabkha) are formed. Figure adapted from Figure 2 of
639   Wood and Imes [51]. Image from Digital Globe to NASA with no restrictions on use or copying.

640
641   Figure 3. Satellite image of the inland sabkha studied here (dark area in the left side of image). The red
642   circle marks the sampling site, GPS coordinates of the sampling site in the center of the sabkha are
643   N23.05088º E53.77005º elevation 86 m. Another interdune flat area is visible about 1 km to the east.
644   North is upward. Image was take on 4 Jan 2015.

645
646   Figure 4. Perspective image of the salt flat surface (background image) with insert of a sampling
647   indentation made to access the water and sediments.

648
649   Figure 5. Close up of an endoevaporite mat. The uppermost white layer, about 5 mm thick, is the salt
650   crust. Below that is a layer, almost 5 mm thick of pink halophilic bacteria and below that a layer of green
651   photosynthetic algae. Below the green layer the material is darker in color. Gas samples were acquired
652   from sediments beneath this mat. The mat pictured above was sectioned from top to bottom as follows –
653   top layer (T) composed of white and pink layer (~0-2 mm from surface); middle layer (M) composed of
654   green layer (~2-4 mm); bottom layer (B) composed of darker brown layer (~4-5 mm); sediment layer (S)
655   mostly composed of fine sand attached to the bottom of the dark brown layer (>5 mm).

656
657   Figure 6. Diagram of the water flow and salt layers of the Liwa inland sabkha. Relatively fresh ground
658   water flows upward into overtopping ancient salt layer. The salt layer inhibits evaporation, increases the
659   salinity of the water near the surface, and allows some sunlight penetration.

660
661   Figure 7. Abundance of bacterial 16S rRNA genes for each phylum for the top, middle, bottom and
662   sediment layers of the mat. All sequences were classified using SINA program, with the exception of the
663   plastids category, which was identified by BLASTN. A plastids category was included along with the
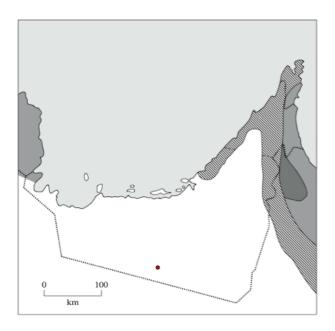664   different phyla, to indicate the presence of phototrophic eukaryotes.
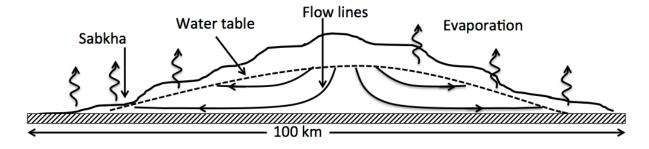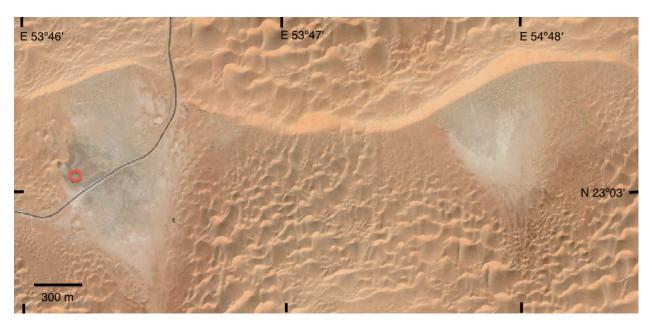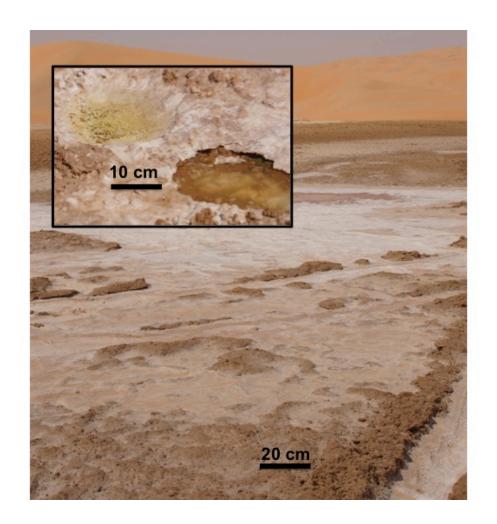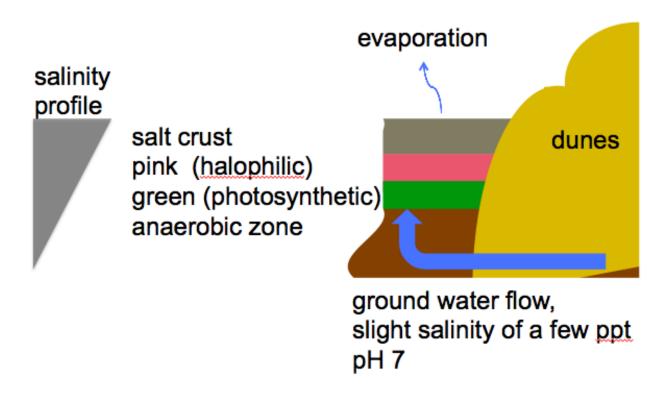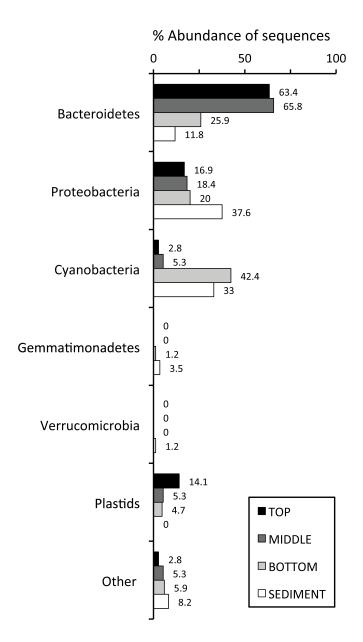
7 Figures

Figure 1.

Figure 2.

Figure 3.

Figure 4.

Figure 5.

evaporation

salinity
profile

salt crust
pink (halophilic)
green (photosynthetic)
anaerobic zone

dunes

ground water flow,
slight salinity of a few ppt
pH 7

Figure 6.

% Abundance of sequences

Figure 7.